Uncertainty Analysis for a Wave Energy Converter: the Monte Carlo Method

Jarrah Orphin[#1], Irene Penesis[#2], Jean-Roch Nader[#3]

[#]*National Centre for Maritime Engineering & Hydrodynamics, Australian Maritime College, University of Tasmania Locked bag 1395, Launceston, Tasmania, 7250, Australia*

[1]jarrah.orphin@utas.edu.au

[2]i.penesis@utas.edu.au

[3]jeanroch.nader@utas.edu.au

Abstract— **Developing wave energy converter technology requires physical-scale model experiments. To use and compare such experimental data reliably, its quality must be quantified through an uncertainty analysis. To avoid uncertainty analysis problems for wave energy converter models, such as providing partial derivatives for time-varying quantities within numerous data reduction equations, we explored the use of a practical alternative: the Monte Carlo method (MCM). We first set out the principles of uncertainty analysis and the MCM. After, we present our application of the MCM for propagating uncertainties in a generic Oscillating Water Column wave energy converter experiment. Our results show the MCM is a straightforward and accurate method to propagate uncertainties in the experiment; thus, quantifying the quality of experimental data in terms of power performance. The key conclusion of this work is that, given the demonstrated relative ease in performing uncertainty analysis using the MCM, experimental results reported in the future literature of wave energy converter modelling should be accompanied by the uncertainty in those results. More broadly, this study aims to precipitate awareness among the wave energy community of the importance of quantifying the quality of modelling data through an uncertainty analysis. We therefore recommend future guidelines and specifications pertinent to uncertainty analysis for wave energy converters, such as those developed by the International Towing Tank Conference (ITTC) and International Electrotechnical Commission (IEC), to incorporate the MCM with a practical example.**

Keywords— **Wave Energy Converter, Experimentation, Uncertainty Analysis, Monte Carlo Method**

I. Introduction

Uncertainty analysis is an indispensable tool in each phase of an experimental program. Its uses include ensuring an experiment can indeed answer a proposed question or set of questions; estimating and using uncertainties in the design, construction, debugging, execution, and data analysis phases; and finally to provide a quantitative indication of the quality of experimental results in the reporting phase [1]. This last use, in essence, makes data meaningful. Without such an indication, not only is it impossible to assess the reliability of results, but these results cannot be compared, either among themselves or with reference values [2]. It is, therefore, apparently obligatory to perform an uncertainty analysis for a wave energy converter (WEC) experiment, if it is to be of scientific or practical value. Strikingly, one rarely encounters evidence of uncertainty analysis in the literature on WEC experimentation. Few studies on this subject have been published [3-5]. Given developing WEC technology toward commercial readiness is requiring multiple stages of physical-scale model experiments [6, 7], with each stage acquiring ostensibly valuable information for due diligence and future technology and business development, this lack of uncertainty analysis evidence is alarming. In the context of the wave energy industry, unknown reliability of experimental results, at bottom, hinders the ultimate goal of reducing levelised cost of energy (LCOE).

A key reason why WEC experimentation literature lacks uncertainty analysis is due to the challenge of modelling a complex WEC system in a complex environment [6, 8]. Oftentimes it is not straightforward to, first, provide a mathematical description of the model and, second, evaluate how variables and their associated uncertainties influence the model's behaviour. In the latter case, such an evaluation requires propagating the uncertainties of each variable through the data reduction equations (DRE's) that describe the model. This task can be difficult or inconvenient when the model contains many variables with multiple DRE's – common for most WECs. While the wave energy community has recently provided general guidance on the principles and use of uncertainty analysis as it relates to WEC experiments [6, 9], treatment of other methods for propagating uncertainty is lacking. In particular, the Joint Committee for Guides in Metrology (JCGM) provides a supplement to the "Guide to the expression of uncertainty in measurement" (GUM) [2] concerned with the propagation of uncertainty using the Monte Carlo method (MCM) [10]. The MCM is a practical alternative to the GUM uncertainty framework based on the law of propagation of uncertainty. It can be applied to overcome various problems in uncertainty evaluation, for example, when the probability density function (PDF) for the output quantity is not a Gaussian distribution; when a model is arbitrarily complex; or when it is difficult or inconvenient to provide the partial derivatives of the model, as needed by the law of propagation of uncertainty.

This paper deals with demonstrating an application of the MCM for evaluating uncertainty in a WEC experiment. The rationale for exploring the use of the MCM in this instance was to overcome difficulty in providing the partial derivatives of an Oscillating Water Column (OWC) wave energy converter model. While we focus on uncertainty analysis in the reporting

of results phase, that is, a post-test uncertainty analysis, the general methodologies presented can be easily adapted for the use of uncertainty analysis in all other phases of a WEC experiment. Moreover, this work may also be applied to uncertainty analysis for numerical models.

The paper is structured as follows. First we provide methodologies of uncertainty analysis according to the guide to the expression of uncertainty in measurement (GUM) uncertainty framework [2], and the MCM [10]. Following this are descriptions of the mathematical model of the OWC WEC and experimental setup. Section III presents the results and our discussion of these results. After, we make a recommendation for the adoption of the MCM in future versions of guidelines and codes on uncertainty analysis for WECs

II. Methodology

There are two primary theoretical considerations of this paper. The first deals with methodologies for evaluating measurement uncertainty through an uncertainty analysis. The second deals with characterising the hydrodynamics and performance of the OWC wave energy converter.

A. Uncertainty analysis

This section sets out, first, the general procedure for evaluating measurement data and expressing uncertainty in measurement [2, 10, 11] and, second, presents our application of these in evaluating measurement uncertainty in an OWC wave energy converter experiment, using the Monte Carlo Method (based on [10] and [1]). For convenience, notation is take from the International Towing Tank Conference (ITTC) guideline 7.5-02-07-03.12 "Uncertainty Analysis for a Wave Energy Converter" [12]. Noted, this section is an extension similar previous work on this subject [5].

The principles of evaluating uncertainty in measurement are categorised into three groups: (a) standard uncertainty, (b) combined uncertainty, and (c) expanded uncertainty. Standard uncertainty is itself grouped into two types: Type A (random uncertainty) and Type B (systemic uncertainty). Combined uncertainty is evaluated using the law of propagation of uncertainty or, as in this paper, through the Monte Carlo Method. Expanded uncertainty is obtained by multiplying combined uncertainty by a coverage factor, typically taken from the Student *t*-distribution (see [13]).

Evaluating Type A standard uncertainty $u_{s\text{-}A}$ is based on statistical analysis. It requires determining the average $\bar{q}$ of a quantity q and the deviation $s(q)$ of its random variation, obtained from n independent observations q_k under the same measurement conditions:

$$\bar{q} = \frac{\sum_{k=1}^{n} q_k}{n} \tag{1}$$

Type A standard uncertainty $u_{s\text{-}A}$ is the experimental standard deviation of the mean $s(\bar{q})$, given by

$$u_{s-A} = s(\bar{q}) = \frac{1}{n}\sqrt{\frac{\sum_{k=1}^{n}(q_k - \bar{q})^2}{n-1}} \tag{2}$$

Type B standard uncertainty $u_{s\text{-}B}$ is evaluated by scientific judgement based on available information on the possible variability of an input quantity X_i. The pool of information may include calibration data or previous measurement data, experience, manufacturers' specifications, uncertainties assigned to reference data, or any other reliable source of information. It is also important to identify and evaluate uncertainties arising in linear models due to nonlinear phenomena. For example, in this experiment we have assumed linear damping, but we can see in Fig. this assumption contains a non-negligible amount of uncertainty, which must be quantified and propagated through the data reduction equations of interest. Hence, it is important to evaluate the significance and quality of each variable of the experiment, where inputs may be measured, assumed, or calculated.

Type B uncertainty in this experiment was evaluated primarily using end-to-end instrument calibration data, by performing a regression analysis to determine the standard error of the estimate SEE:

$$SEE = u_{s-B} = \sqrt{\frac{\left(y_j - \hat{y}_j\right)^2}{M-2}} \tag{3}$$

where and M is the number of calibration points and $y_j - \hat{y}_j$ is the difference between the calibrated data point and the fitted value.

In a similar manner, Type B uncertainty u_B of the hydrodynamic damping coefficient $u_B(\delta)$, assumed to be linear with a linear relationship between pressure p_c and air volume flux Q inside the OWC chamber (Fig. 8), was evaluated through a multivariate normal regression analysis:

$$y_i = X_i\beta + e_i, \quad i = 1, \dots, n, \tag{4}$$

where y_i is the vector of responses, X_i is a design matrix of predictor variables, β is vector of regression coefficients, and e_i is a vector of error terms, with multivariate normal distribution. The error terms (difference between actual and predicted values) are calculated for each independent observation and substituted into Eq. 3 giving a measure of both the repeatability (Type A) and accuracy in the linear damping assumption (Type B).

The standard uncertainty u_s is the combination of Type A and Type B uncertainties through the root-mean-square:

$$u_s = \sqrt{u_{s-A}^2 + u_{s-B}^2} \tag{5}$$

In most cases, the DRE, for example OWC hydrodynamic power, is not measured directly, but is determined from N other (measured or assumed) input quantities X_1, X_2, …, X_N through a functional relationship f:

$$\begin{aligned} &Y = f(X_1, X_2, \dots, X_N), \\ &with\ estimate\ of: y = f(x_1, x_2, \dots, x_N) \end{aligned} \tag{6}$$

The combined standard uncertainty $u_c(y)$ is the positive square root of the combined variance $u_c^2(y)$, given by

$$u_c^2(y) = \sum_{i=1}^{N} \left(\frac{\partial f}{\partial x_i}\right)^2 u^2(x_i) + 2\sum_{i=1}^{N-1}\sum_{j=i+1}^{N} \left(\frac{\partial f}{\partial x_i}\right)\left(\frac{\partial f}{\partial x_j}\right)^2 u_s(x_i, x_j) \quad (7)$$

Eq. 7 is referred to as the law of propagation of uncertainty. The partial derivatives $\partial f / \partial x_i$ (often referred to as sensitivity coefficients) are equal to $\partial f / \partial X_i$ evaluated at $X_i = x_i$; $u_s(x_i)$ is the standard uncertainty associated with the input estimate x_i; and $u_s(x_i, x_j)$ is the estimated covariance associated with x_i and x_j. For cases where estimated quantities x_i are independent and thus uncorrelated ($u_s(x_i, x_j)$~=0), the second term in Eq. 7 can be neglected. For cases where input estimates are correlated, for instance p_c and Q (Fig. 8), the degree of correlation between x_i and x_j is estimated using Pearson's correlation coefficient (see [2]).

Expanded uncertainty U is the combined uncertainty u_s multiplied by a coverage factor k to give an overall uncertainty with a 95% level of confidence. Coverage factor in this investigation was determined using a student T-Distribution [13].

$$U = ku_s \quad (8)$$

Alternatively, the Monte Carlo method may be used to determine the combined uncertainty of a quantity, or of any number of DRE's which are a function of multiple independent and/or correlated quantities, which can themselves be functions of multiple quantities. Among other benefits of using MCM for uncertainty propagation, the method avoids the need to provide partial derivatives of difficult or inconvenient models, as required by the law of propagation of uncertainty. This is the primary reason we have explored its use in this paper.

Drawing on the basic methodology presented in [1], the MCM flow chart shown in Fig. 1 (noted, this methodology assumes $u_{s\text{-}A}$ is calculated for the DRE of interest from multiple observations using Eq. 2). First, the assumed true or nominal values X_{true} of each quantity of a DRE are input. The estimates of the elemental Type B uncertainties $u_{s\text{-}B}$ for each quantity are then input. An appropriate probability distribution function (Gaussian, rectangular, triangular, etc.) is assumed for each error source β_j, with a Gaussian distribution used in this example. For each quantity X_j, random values from a (pseudo)random number generator are assigned to its error source(s). The individual error sources are then summed and added (or subtracted) to the true values of each quantity to obtain "measured" values. Using these measured values, the result of the DRE is calculate.

This process corresponds to running the Monte Carlo simulation once (M = 1). The sampling process is repeated M times to obtain a distribution for the possible DRE result values. From this distribution, mean $\bar{q}_{MCM}$ and standard deviation s_{MCM} statistics can be calculated (s_{MCM} is the combined standard uncertainty u_c of the DRE). The selection of M depends on when the standard deviation has converged (M = 1000 was used in this study, see Fig. 3 for convergence study used to determine M). Typically, convergence of 1-5% is reached after relatively few iterations (< 500). Once a converged value of u_c is obtained, the expanded uncertainty for the result at a 95% confidence level is U = 2 u_c.

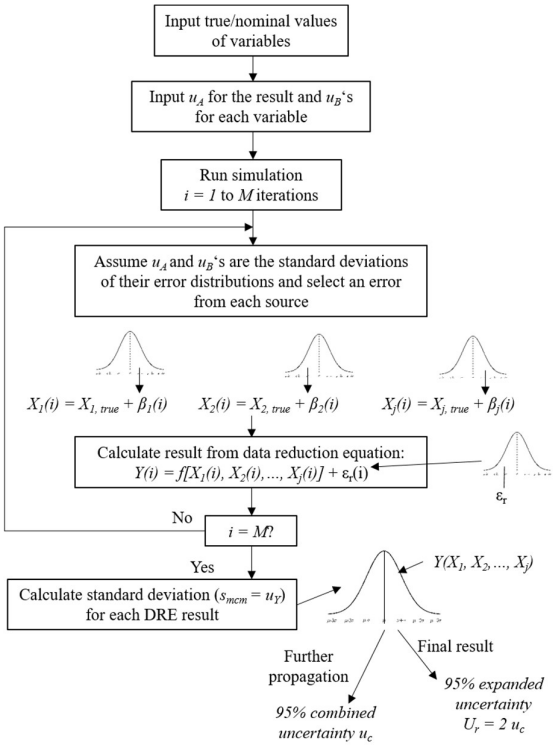

Fig. 1 Schematic of MCM for uncertainty propagation. Directly calculated random standard uncertainty of the data reduction equation, $u_{s\text{-}A}$, is used (shown as random error, ε_r).

B. Mathematical model

1) Hydrodynamic power: In line with previous experiments of a similar nature [9, 11, 12], the air turbine power take-off (PTO) system was assumed to exhibit essentially linear pneumatic damping characteristics; that is, a linear relationship between OWC chamber pressure p_c and air volume flux Q across the turbine, thus representing a Wells turbine [13-16]:

$$\delta = \frac{P_c}{Q} \quad (9)$$

The numerical derivation of volume flux Q (oscillating airflow caused by change in wave elevation inside the chamber) is:

$$Q = \iint_{S_C} \frac{\partial \eta}{\partial t} ds = \iint_{S_C} v_s ds = \bar{v}_s S_c \quad (10)$$

where S_c is the area of the free surface, v_s is the velocity at which the free surface oscillates, and $\overline{v_s}$ is the mean free surface velocity inside the OWC chamber. The instantaneous power P of the OWC is:

$$P(t) = P_c Q \tag{11}$$

The mean power P_h is determined by integrating the instantaneous power over the wave period.

$$P_h = \frac{1}{T}\int_0^T P_c Q \, dt \tag{12}$$

where T is the phase-averaged wave period. By introducing Equation (9) into Equation (12), assuming linear wave theory, the relationship is expressed as:

$$P_{h,\delta} = \frac{1}{T}\int_0^T \frac{P_c^2}{\delta} dt = \frac{1}{2}\frac{A_p^2}{\delta} \tag{13}$$

where A_p is the amplitude of the chamber pressure measured by the pressure sensor.

2) Incident wave power: The regular wave power P_i per device width, assuming intermediate water depth, is calculated as

$$P_i = \frac{1}{T}\int_0^T \frac{1}{2}{\eta_0}^2 \rho g C_g L \tag{14}$$

where η_0 is incident wave amplitude, ρ is water density, g is gravitational acceleration, C_g is the group velocity and L is the wave crest width corresponding to the OWC inlet width.

3) Capture width ratio: Hydrodynamic power P_h is non-dimensionalised by the incident wave power P_i in order to quantify its hydrodynamic efficiency in harnessing incident wave power P_w. This parameter, commonly known as the capture width ratio (CWR), is given by,

$$P_w = \frac{P_h}{P_i} \tag{15}$$

And capture width ratio $P_{w,\delta}$ calculated with OWC power as function of δ:

$$P_{w,\delta} = \frac{P_{h,\delta}}{P_i} \tag{16}$$

C. Experimental setup

The 2D experiments were performed in the Australian Maritime College Towing Tank. This 100 m long, 3.55 m wide, 1.5 m deep tank has a single paddle flap type wave generator at one end and a damping beach at the other. The 1:8 scale, breakwater integrated bent-duct OWC wave energy converter (see [12]) was installed about halfway in the tank (Fig. 2). The OWC model was built into a fully-reflective, flat-faced wall. Refer to Fig. 2 and Table 1 for other further details about the experimental program and parameters.

D. Data processing

Data processing and analysis has been performed following ITTC recommended procedures and guidelines [8, 10, 17, 18], and the Joint Committee for Guides in Metrology (JCGM) with their guide to the expression of uncertainty in measurement (GUM) framework [2, 7]. Time series data were trimmed such that data used for analysis contained only that which was considered stationary (see Fig. 5).

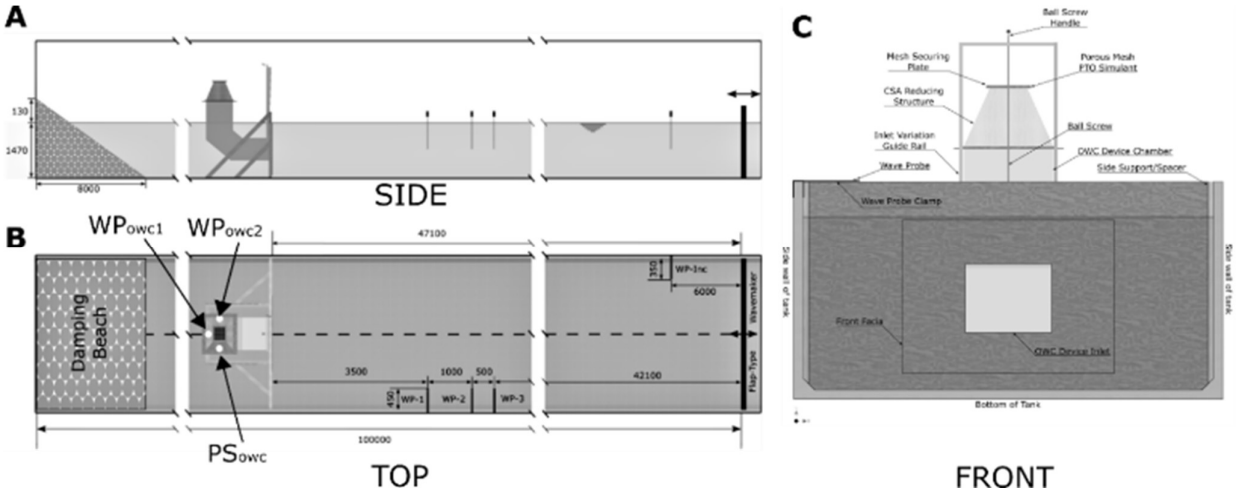

Fig. 2 Drawings of 1:8 scale OWC wave energy converter integrated into a flat-faced breakwater showing **A** side, **B** top and **C** front views. This model was tested in the Australian Maritime College Towing Tank.

TABLE I
EXPERIMENTAL PROGRAM AND PARAMETERS

Parameter	Details
Model	1:8 scale breakwater integrated OWC wave energy converter, with linear PTO damping simulated using porous mesh cloth (Enviro-Cloth).
Water depth	1.47 m
Waves	Long-crested regular waves: H = 0.05 m, f = 0.3 – 0.45 Hz.
Measurement Instruments	Incident wave probe, WP_{inc} OWC wave probe 1, WP_{owc1} OWC wave probe 1, WP_{owc2} OWC pressure sensor, PS_{owc} (Honeywell Controls TruStability)
Conditions	6 x linear PTO damping values: $\delta_1 \sim= 1237$ Nsm^{-5} $\delta_2 \sim= 2390$ Nsm^{-5} $\delta_3 \sim= 3482$ Nsm^{-5} $\delta_4 \sim= 4607$ Nsm^{-5} $\delta_5 \sim= 5412$ Nsm^{-5} $\delta_6 \sim= 6497$ Nsm^{-5}

E. Monte Carlo method for uncertainty propagation

Here we present a graphical presentation of the Monte Carlo method simulation setup for propagating uncertainties, applied to a generic OWC wave energy converter experiment (fig. 4A), and the MCM simulation output of expanded uncertainty of quantities and DRE's fig. 4E). Illustrated in fig. 4A are the nominal inputs for each quantity (measured or assumed), their associated standard uncertainties (evaluated or assumed), and the DREs required to calculate the final result of capture width ratio P_w. Assumed nominal and uncertainty values have been taken from standard reference materials. Some quantities (*S, g, h, ρ* and *L)* are wave independent, whereas the remaining quantities are wave dependent. figs. 4B, C, D show exemplar results (i = 1, H = 0.05 m, f = 0.34 Hs, $\delta_5 \sim= 5412$ Nsm^{-5}) of propagating quantities that are not single values, but time series. For each simulation i, the basic method is that of multiplying each individual data point of the selected time series with a random number, taken from a normal distribution N.

The MCM was applied because most quantities are inherently transient in typical WEC experiments, due to waves. This leads to difficulty in evaluating and propagating uncertainties. For example, propagating uncertainties through integral functions is not practical using the law of propagation of uncertainty, because one must provide the standard uncertainty for each measured and influence quantity, and partial derivatives of each DRE, some of which themselves become variables in higher-level DRE's, for example Cg. In contrast, it can be seen that the MCM provides a straightforward way in which to propagate uncertainties; only the DRE and the standard uncertainty associated with each quantity have to be provided.

To glimpse what the outputs of a MCM uncertainty propagation looks like, expanded uncertainty functions of primary DRE's – incident wave power P_i, OWC power P_h, and capture width ratio P_w – are given (fig. 4E). Also included are example results of OWC power P_h and its constituents (P_c, Q), after M = 1000 simulations. fig. 4F, H, J show the mean value (black line) and the variation of each data point (grey dots). fig. 4G, I, K show the histogram of peak amplitude values, including the mean (black line) and expanded uncertainty to a 95% confidence interval with k = 2 (black dashed lines). These peak amplitude uncertainty values are reported as the final uncertainty associated with final result statements.

To determine how many iterations of the MCM simulation are necessary, a convergence study must be conducted (fig. 3). Convergence is determined by calculating at each iteration the combined standard deviation s_{MCM} of a DRE of interest, for example OWC power P_h. Subsequently plotting s_{MCM} shows the convergence behaviour. From fig. 3 it may be seen that after only 300 iterations the value has converged to within 2% of the fully converged value. We repeated this process for all primary DRE's, and deemed that after 100 iterations the values were fully converged.

As one may see, performing a pre-experiment uncertainty analysis using the MCM would be also be relatively straightforward, by assuming nominal values and analytical wave signals with estimated elemental uncertainties

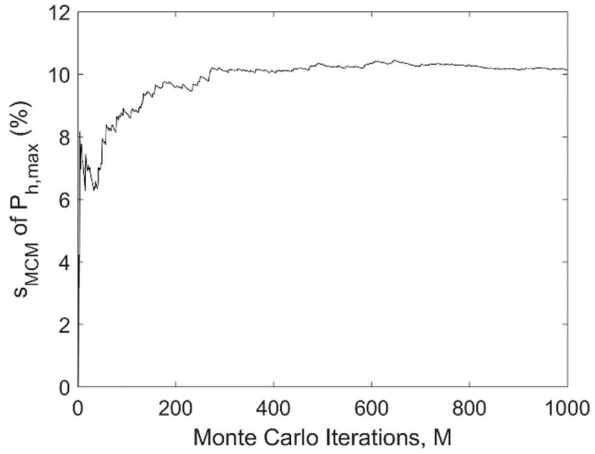

Fig. 3 Convergence of expanded uncertainty U ($2.s_{MCM} = U$) of OWC power P_h.

III. RESULTS & DISCUSSION

We report the results and discuss them in three parts. First, time series data show how data were trimmed in the stationary region for analysis, as well as provide an indication of the repeatability of experimental runs. Second, uncertainty of measured quantities is presented and, third, results for the propagation of uncertainty using the MCM. Throughout this section, while we report and discuss the results of dependant variables in their context, we do so only briefly; the focus is on reporting and discussing uncertainty results. Uncertainty results reported are those calculated at the peak amplitude quantities and data reduction equations, to a 95% confidence interval (CI).

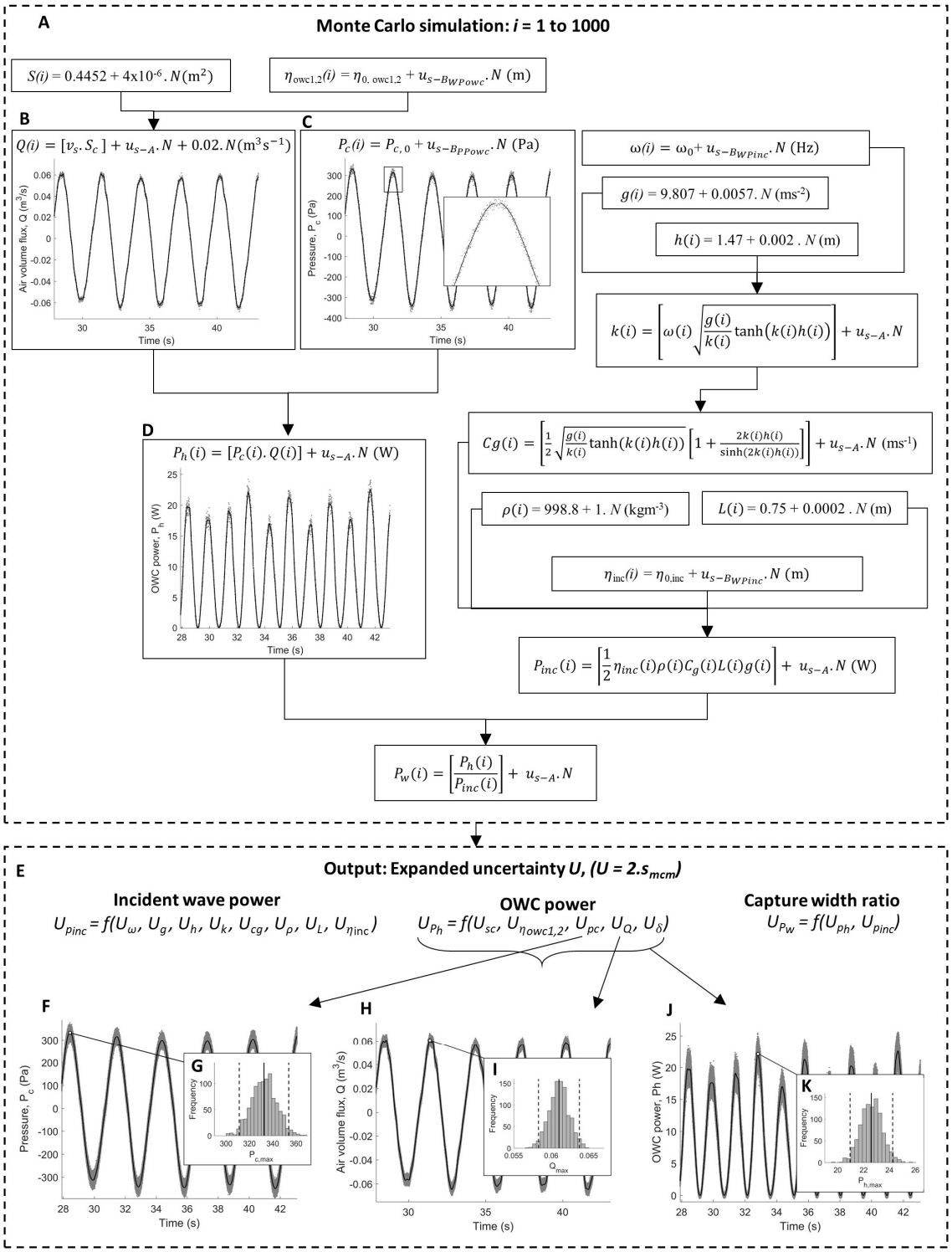

Fig. 4 A graphical representation of the Monte Carlo method for propagating uncertainties in a generic OWC wave energy converter experiment. **A**, MCM simulation (M = 1000), with example results of time-variant quantities of OWC power P_h for i = 1, with black profiles being the actual time series and the grey dots the standard uncertainty multiplied by a random number taken from a normal distribution N. (**B, C, D**). **E**, MCM simulation output: expanded uncertainty U (95% confidence interval) of each quantity and data reduction equation, with example results plotted for i = 1:M (**F, H, J**). **G, I, K,** histogram subplots showing the mean (black line) and expanded uncertainty (dashed lines) of $P_{c,max}$, Q_{max} *and* Ph_{max} respectively. Example results are H = 0.05 m, f = 0.34 Hs, δ_5 ~= 5412 Nsm^{-5}.

A. *Time series*

Selected repeat experimental runs of one wave condition (H=0.05 m, f=0.45 Hz) indicate minor observed variation in both magnitude and phase for measured quantities (Fig. 5). Incident wave profiles in Figs. 5A, B, and C include one run for each of the six damping conditions (coloured lines) along with nine dedicated repeat runs (black lines). The standard deviation of the mean (Type A standard uncertainty u_A) for wave height H and period T, determined from each individual wave defined by the zero-up crossing, was 0.0008 m and 0.0008 s respectively. While in general the profiles show sinusoidal characteristics, there are slight nonlinearities observed in the first three waves of the trimmed time series profiles. It is assumed these nonlinearities have a negligible influence on the primary wave parameters of H and T.

Measurements inside the OWC chamber of pressure p_c and surface elevation η_{owc} in Figs. 5D, E, and F include nine dedicated repeat runs. Similarly, these results indicate only slight variation and, in effect, are highly repeatable experimental runs for this wave condition. There are minor nonlinearities observed in the p_c profiles around the zero crossing, which may be attributed to a physical effect in the hogging and sagging of the damping simulator (porous mesh material) after η_{owc} reaches its maximum and begins to fall causing a positive-negative change in p_c. Wave probes inside the OWC chamber WP_{owc1} and WP_{owc2} evidently measured similar η_{owc} quantities, indicating the free surface inside the chamber was essentially level during its cycle. This confirms the validity in the flat-plate assumption used to numerically derivate air volume flux Q. Noted, wave frequencies around resonance exhibited up to 10% variation between η_{owc1} and η_{owc2}, which hinders the said assumption, however this uncertainty is accounted for in the standard error of the estimate of the pneumatic damping coefficient.

B. *Uncertainty of measured quantities*

To quantify the uncertainty of measured quantities, we first evaluated standard uncertainty components and then used the MCM to combine these standard uncertainties, giving the expanded uncertainty. For each of the measured quantities in the experiment, expanded uncertainties U were less than 10% on average, with Type A $u_{S\text{-}A}$ and Type B $u_{S\text{-}B}$ standard uncertainties less than three percent on average (Fig.). All $u_{S\text{-}A}$ results for measured quantities contained outliers, the maximum of which reached five percent. Looking at $u_{S\text{-}B}$ results, we can see that all the data fall below 2.5% uncertainty. These results are very similar to those presented in [5] and the example in [12], with the exception of $u_{S\text{-}B}(p_c)$ in this experiment, which had a smaller uncertainty of 2.5%, with 0.5% arising from calibration data of PS_{owc}, and 2% assumed to account for for the uncertainty of the instrument used to calibrate the pressure sensor. In comparison, $u_B(p_c)$ in [5] was ~ 5%. This reduced $u_B(p_c)$is a consequence of testing at a larger scale of 1:8 (compared with 1:20), such that the calibration range of PS_{owc} for the 1:8 scale was larger and thus the variation relatively smaller.

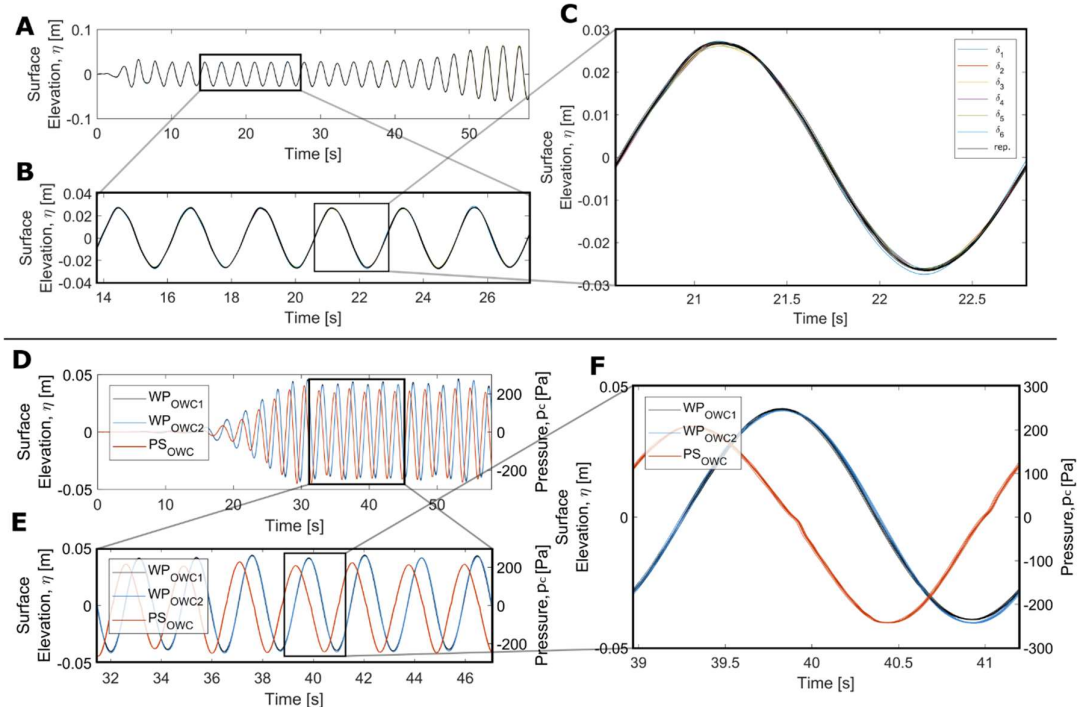

Fig. 5 **A-E**, Synchronised time series profiles of repeated runs (overlayed) of one wave condition (H=0.05 m, f=0.45 Hz). **A**, incident wave surface elevation, η_{inc}; **B**, cropped data in the stationary region; **C**, a crop of one incident wave to aid examination of the repeatability of incident waves; **D**, surface elevation inside the OWC chamber, $\eta_{owc1,2}$, measured by wave probes $WP_{owc1,2}$ (left axis), and pressure inside the OWC chamber, p_c (right axis); **E**, cropped data in the stationary region, used in the analysis; and **F**, a crop of one wave showing repeatability and relation of p_c and $\eta_{owc1,2}$ inside the OWC chamber.

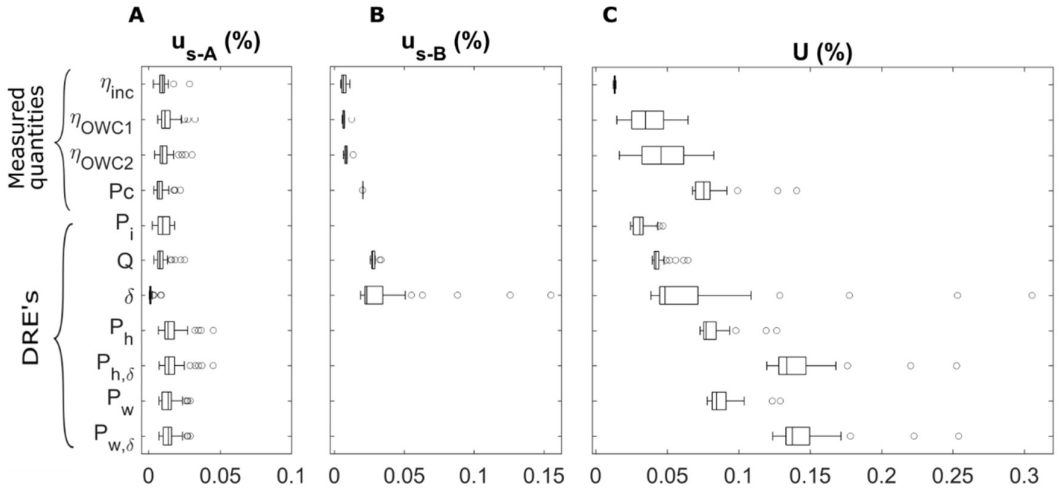

Fig. 6 Uncertainty analysis results, including **A** Type A $u_{s\text{-}A}$, **B** Type B $u_{s\text{-}B}$, and **C** expanded uncertainty U. Boxplots represent uncertainty results for each experimental run of each condition, with normal convention (box = median with 25th and 27th percentiles, whiskers = extreme points not considered outliers, circles = outliers. **B**, sensor calibration data constitutes $u_{s\text{-}B}$ for measured quantities, whereas $u_{s\text{-}B}$ for δ is the systematic uncertainty in the linear damping assumption. **C**, U is to 95% CI, with k varying depending on n of each respective experimental run.

C. *Uncertainty of data reduction equations*

Uncertainty results for the data reduction equation's (DRE's) of interest were generally larger compared with measured quantities' uncertainty (Fig.). In terms of standard uncertainty, $u_{S\text{-}A}$ was always smaller than $u_{S\text{-}B}$. The largest $u_{S\text{-}B}$ result was observed in pneumatic damping δ, with approximately four percent uncertainty on average, and a maximum of 15%. This result was primarily due to the systematic uncertainty arising from the linear damping assumption (Eq. 4). Air volume flux Q showed an approximate three percent $u_{S\text{-}B}$ value, with this $u_{S\text{-}B}$ uncertainty component being a combination of the OWC wave probes' calibration data (see Eq. 10) and an assumed 2% uncertainty to account for the piston assumption of water elevation inside the OWC chamber. There were no $u_{S\text{-}B}$ components estimated for incident wave power $P_{i,}$ OWC power $P_{h,}$, OWC power $P_{h,\delta}$ as function of δ, capture width ratio P_w, or capture width ratio $P_{w,\delta}$ as function of δ, as these are functions of other DRE's and quantities. Noted, $P_{h,\delta}$ and $P_{w,\delta}$ are the result of calculating OWC power using Equation 13, with $P_{h,\delta}$ being a function of P_c and δ, and then using this $P_{h,\delta}$ to calculate capture width ratio $P_{w,\delta}$ as function of δ. These power calculations with δ are useful for scaling up power results and associated uncertainty, as they take into consideration the linear damping assumption.

Expanded uncertainty U results for DRE's were less than ~15% on average. However, some values of δ, $P_{h,\delta}$ and $P_{w,\delta}$ reached 25-30%. $P_{w,\delta}$ showed largest overall expanded uncertainty, as expected considering it is a function of both OWC and wave power. $P_{h,\delta}$ and $P_{w,\delta}$ calculations as a function of δ and P_c (Equation 13) were larger compared with P_h and P_w, due to δ having a large Type B uncertainty. In the context of relevant work [5], where an experiment was conducted on a 1:20 scale model version of the 1:8 scale model investigated here, these expanded uncertainty results are less than half of those reported in previous work, for reasons discussed above.

To further the analysis of uncertainty in the primary DRE's – incident wave power, OWC power and capture width ratio – we then plotted the results of each experimental condition across the wave frequency range tested (Fig.). The following sections report on these results and discuss their significance.

(1) Incident wave power: Incident wave power P_i decreased monotonically as wave frequency increased, and the uncertainty associated with these results was less than 5% on average (Fig. A). Of this, ~60% was due to the measurement of the incident wave elevation η_{in}, with the other four variables of P_i making up the remaining ~40% (Fig. B). Slight variation of incident wave power was observed between experimental conditions ($\delta_{1\text{-}6}$) of the same wave condition, evident in different magnitudes for a particular wave frequency. The largest difference in magnitude was observed to be 5%. Interestingly, there was also a systematic difference in magnitude between experimental runs for the frequency range tested. This is observed by inspecting, for example, δ_4 (square marker) and δ_5 (diamond marker) where P_i for δ_5 is always larger than δ_4, by ~2% on average. This illuminates a systematic error in the experiment; the measurement of η_{in} is the predominant source of this systematic error, which we infer is due to experimental runs being conducted on different days, and therefore subject to a separate calibration set.

2) OWC hydrodynamic power: The effect of pneumatic damping on OWC power was observed to be significant around the resonance frequency of the WEC, both in terms of magnitude and the broadness of the response spectrum (Fig. C). At the resonant frequency of f = 0.37 Hz, $P_{h,\delta}$ for the lightest damping condition δ_1 was approximately twice the value observed for the heaviest damping condition δ_6. In general, the heavier the damping, the lower the $P_{h,\delta}$, except at ~0.1 Hz either

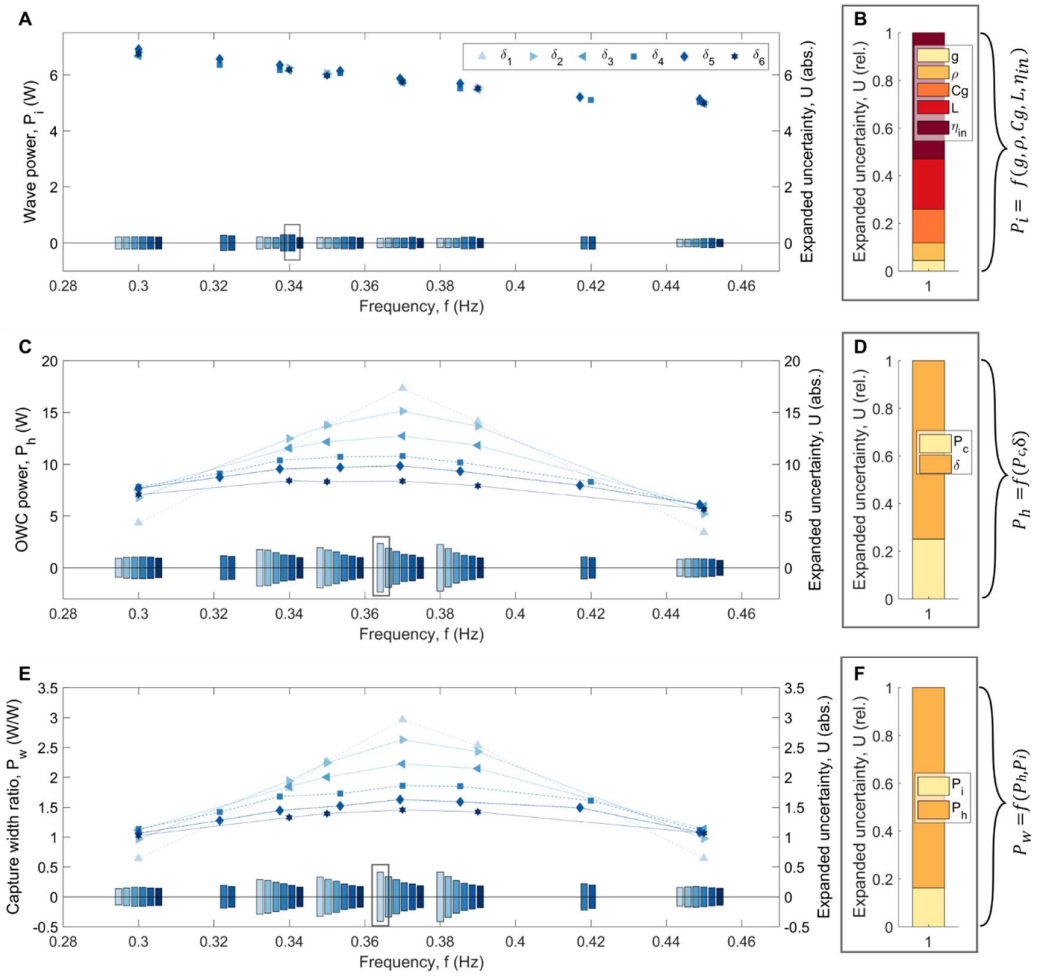

Fig. 7 Main data reduction equation (DRE) results (left axes) with associated expanded uncertainty (right axes), evaluated using the Monte Carlo method (95% CI, $k = 2$). **A**, Incident wave power P_i, with **B** showing the proportion of each quantities' uncertainty within the P_i DRE; the maximum observed uncertainty of P_i is selected to show by example (box on bar plot). **C**, OWC power P_h, with **D**, proportions of maximum uncertainty. **E**, Capture width ratio P_w, with **F**, proportions of maximum uncertainty.

side of the peak, where this trend begins to reverse, due to the peakier behaviour of light damping. In terms of the power response spectrum, increasing damping increased the broadness of the spectrum across the frequency range.

Uncertainty results (bar plots) for $P_{h,\delta}$ showed a trend of increasing absolute uncertainty with increasing magnitude of $P_{h,\delta}$. This trend agrees with findings of a similar study [5]. The largest observed uncertainty of 17.8% occurred at the resonant frequency for the δ_1 condition. Fig. D shows that of this 17.8%, ~80% of the uncertainty was due to δ, and ~20% due to P_c.

Fig. shows the damping results for each condition, whereby P_c and Q are plotted against each other, from which the uncertainty in the linear damping assumption be visualised. From Eq. 9, theoretical δ is calculated from the ratio of p_c and Q; however, experimentally δ is determined by taking the gradient of the multivariate linear regression line of p_c vs. Q. This damping coefficient is assumed to be frequency independent; thus, it represents the damping on the system for all frequencies tested for that damping condition. Evident in Fig. , however, is nonlinear behaviour exhibited by p_c and Q. The nonlinearity generally increased with decreasing δ, that is, fewer number of porous mesh damping simulators. The SEE of the smallest δ ($\delta = 1237\ Nsm^{-5}$), corresponding to one layer of damping mesh, was on average 8.5%, with maximum 15.0%, and minimum 5.5%. This variation can be attributed to a physical effect where the mesh damping simulator does not exhibit completely rigid characteristics, rather it hogs and sags slightly due to p_c and Q driven by η_{owc}. This linear damping uncertainty is considered a Type B uncertainty, and is propagated as such through the hydrodynamic power P_h DRE using the MCM.

4) Capture width ratio: The trends and uncertainty results of p_w are similar to those of $P_{h,\delta}$ (Fig. E). This was expected due to P_i's linear decreasing trend. It can be see that $P_{w,\delta}$ reaches up to a value of three. Put another way, the breakwater integrated WEC is harnessing three times the incident wave energy, due to reflection and resonance. The uncertainty results are very similar to those of $P_{h,\delta}$, due to P_i uncertainty making up

approximately one third of $P_{w,\delta}$'s total uncertainty. These results compare favourably to similar work [5]; however, it is assumed these results are more accurate in describing the overall uncertainty of the presented DRE's due to using the integral of the phase-averaged result rather than simply the mean of the amplitude. In this way, the uncertainty in nonlinear behaviour is captured and propagated through the DRE's.

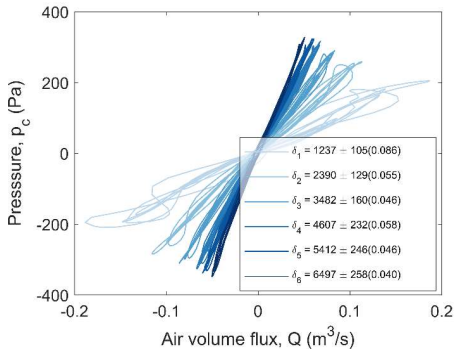

Fig. 8 P_c vs. Q, showing the damping δ for each condition ($\delta_{1\text{-}6}$) and the associated Type B uncertainty determined through linear regression (Eq. 6).

IV. Conclusions

To avoid uncertainty propagation problems, such as providing partial derivatives for complex models with many time-varying variables and data reduction equations, we explored using the Monte Carlo method as a practical alternative for uncertainty analysis. We provided the principles of uncertainty analysis and the methodology of a MCM uncertainty analysis, along with a graphical representation and demonstration of propagating uncertainties of time-varying quantities.

Standard and overall uncertainty results for measured quantities in the experiment were presented. Standard uncertainty results – Type A and Type B – averaged less than three percent to a 95% confidence interval. These uncertainties along with other influence quantities were propagated through the DRE's related to OWC power performance. Incident wave power expanded uncertainty across all frequencies testing averaged less than five percent. The largest expanded uncertainty for pneumatic damping was 31% for δ_1, corresponding to one layer of porous mesh, with a mean of 8.6%. Hydrodynamic power and capture width ratio showed similar result trends and expanded uncertainties, with a maximum of ~18% observed for δ_1 condition.

While we focused only on a post-experiment MCM uncertainty analysis (reporting phase), the general methodology may be applied to pre- and during-experiment phases, including planning, design, debugging, construction, execution, and data analysis. Moreover, the MCM is a suitable and straightforward way in which to perform an uncertainty analysis on complex WEC models. Therefore, we recommend future guidelines and codes pertinent to uncertainty analysis for WECs, such as those developed by the International Towing Tank Conference (ITTC) and international Electrotechnical Commission (IEC), to incorporate the MCM and provide a simple practical example.

In future work we intend on investigating the use and usefulness of pre-test uncertainty analysis using the Monte Carlo method.

Acknowledgment

We thanks the AMC staff, technicians, and students for their contribution of this work.

References

1. Coleman, H.W. and W.G. Steele, *Experimentation, validation, and uncertainty analysis for engineers*. 2009: John Wiley & Sons.
2. JCGM, *Evaluation of measurement data—Guide to the ex pression of uncertainty in measurement*, in *JCGM 100:2008*. 2008.
3. ITTC, *Wave Energy Converter Model Test Experiments*, in *7.5-02-07-03.7*. 2017, International Towing Tank Conference
4. Holmes, B., *Tank Testing of Wave Energy Conversion Systems*. 2009, EMEC: UK.
5. McCombes, T., C.M. Johnstone, B. Holmes, L.E. Myers, A.S. Bahaj, and J.P. Kofoed, *Best practice for tank testing of small marine energy devices*. 2010, EquiMar.
6. JCGM, *Evaluation of measurement data — Supplement 1 to the "Guide to the expression of uncertainty in measurement" — Propagation of distributions using a Monte Carlo method*, in *JCGM 101:2008*. 2008.
7. JCGM, *Evaluation of measurement data — Supplement 2 to the "Guide to the expression of uncertainty in measurement" — Extension to any number of output quantities*, in *JCGM 102:2011*. 2011.
8. ITTC, *Uncertainty Analysis for a Wave Energy Converter* in *7.5-02-07-03.12*. 2017, International Towing Tank Committee.
9. Orphin, J., J.-R. Nader, I. Penesis, and D. Howe, *Experimental Uncertainty Analysis of an OWC Wave Energy Converter*, in *European Wave and Tidal Energy Conference*. 2017a: Cork, Ireland.
10. ITTC, *Guide to the Expression of Uncertainty in Experimental Hydrodynamics*, in *7.5-02-01-01* 2014, International Towing Tank Conference.
11. Howe, D., J.-R. Nader, J. Orphin, and G. Macfarlane, *The Effect of Lip Extrusion on Performance of a Breakwater Integrated Bent Duct OWC WEC*, in *European Wave and Tidal Energy Conference*. 2017: Cork, Ireland. .
12. Howe, D. and J.-R. Nader, *OWC WEC integrated within a breakwater versus isolated: Experimental and numerical theoretical study.* International Journal of Marine Energy, 2017.
13. Nader, J.-R., S.-P. Zhu, P. Cooper, and B. Stappenbelt, *A finite-element study of the efficiency of arrays of oscillating water column wave energy converters.* Ocean Engineering, 2012. **43**: p. 72-81.
14. Evans, D.V. and R. Porter, *Efficient calculation of hydrodynamic properties of OWC-type devices.* Journal of Offshore Mechanics and Arctic Engineering, 1997. **119**(4): p. 210-18.
15. Howe, D. and J.R. Nader, *Experimental and Numerical Theoretical Study of a Breakwater Mounted OWC Wave Energy Converter.* International Journal of Marine Energy, 2017. **17**: p. (Submitted Pending Acceptance).
16. Sheng, W. and A. Lewis, *Wave energy conversion of oscillating water column devices including air compressibility.* Journal of Renewable and Sustainable Energy, 2016. **8**(5): p. 054501.
17. ITTC, *Analysis Procedure for Model Tests in Regular Waves* in *7.5-02-07-03.2*. 2017, International Towing Tank Conference
18. ITTC, *Uncertainty Analysis Instrument Calibration* in *7.5-01-03-01*. 2014, International Towing Tank Conference
19. Fleming, A., *Phase-averaged analysis of an oscillating water column wave energy converter*, in *National Centre for Maritime Engineering and Hydrodynamics*. 2012, Australian Maritme College University of Tasmania.
20. López, I., B. Pereiras, F. Castro, and G. Iglesias, *Performance of OWC wave energy converters: influence of turbine damping and tidal variability.* International Journal of Energy Research, 2015. **39**(4): p. 472-483.